Astron. Astrophys. 293, 293–308 (1995)

ASTRONOMY AND ASTROPHYSICS

A snapshot of the continuous emission of the active galactic nucleus in NGC 3783 from gamma-ray to radio wavelengths*

D. Alloin,[1] M. Santos-Lleó,[1] B.M. Peterson,[2] W. Wamsteker,[3] B. Altieri,[4] W. Brinkmann,[5] J. Clavel,[4] D.M. Crenshaw,[6,7] I.M. George,[8,9] I.S. Glass,[10] W.N. Johnson,[11] G.A. Kriss,[6,12] M.A. Malkan,[13] R.S. Polidan,[14] G.A. Reichert,[6,9] P.M. Rodríguez-Pascual,[3] W. Romanishin,[15] C.H. Starr,[16,9] G.M. Stirpe,[17] M. Taylor,[18] T.J. Turner,[8,9] H. Vega,[19] C. Winge,[20] and D.O.S. Wood[21]

[1] Observatoire de Paris, URA 173 CNRS, F-92195 Meudon, France
[2] Department of Astronomy, Ohio State University, 174 West 18th Avenue, Columbus, OH 43210, USA
[3] ESA – IUE Observatory, Vilspa, Apartado 50727, E-28080 Madrid, Spain
[4] ISO Observatory, Astrophysics Division of ESA, ESTEC, Postbus 299, NL-2200-AG Noordwijk, The Netherlands
[5] Max-Planck-Institut für Extraterrestrische Physik, Giessenbachstrasse, D-85740 Garching, Germany
[6] Guest Observer with the *International Ultraviolet Explorer* Satellite
[7] Science Programs, Computer Sciences Corporation, NASA Goddard Space Flight Center, Code 681, Greenbelt, MD 20771, USA
[8] Laboratory for High Energy Astrophysics, NASA Goddard Space Flight Center, Code 668, Greenbelt, MD 20771, USA
[9] Universities Space Research Association, Code 668, NASA Goddard Space Flight Center, Greenbelt, MD 20771 USA
[10] South African Astronomical Observatory, P.O. Box 9, Observatory 7935, South Africa
[11] E.O. Hulburt Center for Space Research, Naval Research Laboratory, Code 7651, 4555 Overlook NW, Washington, DC 20375, USA
[12] Department of Physics and Astronomy, Johns Hopkins University, Baltimore, MD 21218, USA
[13] Department of Astronomy, University of California at Los Angeles, Math-Science Building, Los Angeles, CA 90024, USA
[14] Laboratory for Astronomy and Solar Physics, NASA Goddard Space Flight Center, Code 681.0, Greenbelt, MD 20771, USA
[15] Department of Physics and Astronomy, University of Oklahoma, Norman, OK 73019, USA
[16] CGRO Science Support Center, NASA Goddard Space Flight Center, Greenbelt, MD 20771, USA
[17] Osservatorio Astronomico di Bologna, Via Zamboni 33, I-40126 Bologna, Italy
[18] Catholic University of America, Washington DC 20064, USA
[19] European Southern Observatory, La Silla, Casilla 19001, Santiago, Chile
[20] Departamento de Astronomia, Instituto de Física, Universidade Federal do Rio Grande do Sul, Avenida Bento Gonçalves, 9500, CP15051, CEP 91500, Porto Alegre, RS, Brazil
[21] National Radio Astronomy Observatory, P.O. Box 0, Socorro, NM 87801, USA

Received 7 April 1994 / Accepted 4 July 1994

Abstract. With the aim of better understanding the physical processes that produce the continuous emission in active galactic nuclei (AGNs), a snapshot of the overall continuous energy distribution of NGC 3783, from γ-ray to radio wavelengths, has been obtained within the framework of the World Astronomy Days. The data collected in this campaign are from GRO, ROSAT, Voyager 2, IUE, HST, ESO, CTIO, SAAO and the VLA. Great care has been taken in disentangling the genuine AGN continuous emission from other contributions: depending on the waveband, the latter might be (i) unrelated contaminating sources in cases where the instrument field of view is large, (ii) components within which the AGN is embedded, such as the stellar bulge population which accounts for a significant fraction of the optical continuum, and free-bound and FeII blends which contribute to the ultraviolet flux. After correction for these other contributions, the continuous emission of the isolated AGN appears to be rather flat (i.e., approximately equal energy per unit logarithmic frequency) from soft γ-ray to infrared wavelengths. At high energies (0.1 MeV to 0.1 keV), the AGN continuum can be fitted by a power law $F_\nu \propto \nu^{-\alpha}$ with a spectral index $\alpha \approx 1$. At longer wavelengths, two excesses above this power law ("bumps") appear: in the ultraviolet, the classical big blue bump, which can be interpreted as thermal emission from the accretion disc surrounding a massive black hole, and in the infrared a second bump which can be ascribed to thermal emission from dust in the vicinity of the AGN, heated by ultraviolet radiation from the central source. By fitting accretion-disc models to the observed AGN spectral energy distribution, we find values for the accretion disc innermost temperature, accretion rate, and

Send offprint requests to: D. Alloin

* Based on observations with the GRO (NASA), ROSAT (DARA/NASA/SERC), Voyager (NASA), HST (NASA/ESA) and IUE (NASA/ESA/SERC) spacecraft and at ESO (La Silla), CTIO, SAAO, and VLA

black hole mass, with some differences that depend on whether or not we extrapolate the high-energy power law up to infrared wavelengths. A fit to the IR bump above the extended $\alpha = 1$ power law suggests the presence of a dust component covering the region from a distance $r \approx 80$ light days (hot grains at a temperature $T \approx 1500$ K) to $r \approx 60$ light years (cool grains at $T \approx 200$ K). The total mass of dust is around 60 $M_\odot$.

Key words: galaxies: Seyfert – galaxies: individual: NGC 3783 – galaxies: nuclei – radiation mechanisms: non-thermal – radiation mechanisms: thermal – black hole physics

1. Introduction

Active galactic nuclei (hereafter AGNs) are known to emit a large amount of energy, typically in the range 10^{33-41} watts, with two specific characteristics which make them unique: (i) the energy is distributed at all frequencies from gamma rays to radio wavelengths, and (ii) the energy output varies with time, on different time scales for different wavebands, and more rapidly at higher energies. Gravitational energy release is usually invoked to explain both short time-scale variability at high energies and the large overall luminosity of AGNs, although the specifics of physical processes involved remain obscure. In order to disentangle the various physical mechanisms that contribute to the observed spectra and thus to form a consistent picture of the origin of their overall continuous emission, it is therefore necessary to observe AGNs over the entire electromagnetic spectrum and to monitor their variations in each of the wavebands. From an observational point of view, this is an extremely ambitious goal. However it is clearly the next important step to be made if we wish to make progress in the understanding of the physics of AGN.

Over the last several years, continuum and emission-line variability has been used to explore the size and structure of the central regions of AGNs. By following the response of the broad emission lines to changes in the continuum, which is generally supposed to arise in an accretion disc surrounding a supermassive black hole, it is possible to determine the structure of the so-called broad-line region (BLR). Reverberation mapping techniques (see Peterson 1993) have been applied to derive, from the delays between the light curves of the UV continuum and the BLR line emission, information about the size and spatial organization of the BLR gas. Following the early studies of NGC 4151 (Clavel et al. 1990 and references therein), large international coordinated monitoring campaigns have been established to collect well-sampled data sets, both in the UV (with both IUE and HST) and in the optical domains. Some of the largest multiwavelength programmes have been carried out by a consortium known as the International AGN Watch (Alloin et al. 1994). The first AGN Watch programme was an extensive IUE/ground-based campaign on the Seyfert 1 galaxy NGC 5548 (Clavel et al. 1991; Peterson et al. 1991, 1992, 1994; Maoz et al. 1993; Dietrich et al. 1993).

In addition to providing information on the size and structure of the BLR, these campaigns have produced important results on the nature of the continuum emission as well. Comparison of the UV and optical data reveals that to the time resolution of the data (between one and four days, depending on the campaign), there is no measurable time delay between the UV and optical continuum variations. This result places stringent constraints on accretion-disc models that must be considered in the interpretation of the continuous emission from these AGNs. Similar constraints on the more energetic γ-ray and X-ray emission could be especially enlightening. Because AGNs vary on different timescales in different wavebands, a useful first step is to obtain a "snapshot" of the overall continuum spectral energy distribution, i.e., contemporaneous multiwavelength observations of a single AGN. In addition to constraining the accretion-disc model and providing a consistent picture of the continuous radiation, these data would also allow us to probe more directly the shape of the radiation field, which is information required for the photoionization equilibrium codes that are currently used to interpret the BLR and narrow-line region (NLR) emission in AGNs.

During 1991–92, the International AGN Watch consortium carried out a large campaign to monitor the UV and optical variability of the AGN in NGC 3783. This galaxy is an almost face-on spiral (SBa), at a redshift of $z = 0.0097$ and with overall size around 110″. It hosts a Seyfert 1 nucleus which has been extensively studied in X-rays (Marshall et al. 1981; Reichert et al. 1985; McHardy 1988; Turner et al. 1991; Ghosh et al. 1992), the UV (Marshall et al. 1981; Barr et al. 1983; Chapman et al. 1985) and the optical/near-IR (Pelat et al. 1981; Menzies & Feast 1983; Stirpe et al. 1988; Evans 1989; Winge et al. 1992; Winkler et al. 1992; Glass 1992). The AGN Watch campaign took place from 1991 December 21 to 1992 July 29 in the UV (IUE), and from 1991 December 3 to 1992 August 9 in the optical (Reichert et al. 1994, AGN Watch Paper V; Stirpe et al. 1994, AGN Watch Paper VI). An opportunity to obtain a snapshot of the overall continuous distribution of NGC 3783 occurred in the framework of the World Astronomy Days (hereafter WAD), an ESA sponsored activity in the context of the International Space Year that was established to coordinate on a worldwide basis the use of many facilities on a chosen target. Through this channel and the cooperation of many observers, we were able to obtain nearly simultaneous data on the AGN in NGC 3783 from γ-ray to radio wavelengths. The primary date chosen for the WAD observations was 1992 June 29 (JD 2448802.5). However, difficulties in scheduling some of the space-based observations led to another set of observations which were made on a secondary date (1992 July 27 = JD 2448830.5). The facilities involved in the WAD campaign were the Compton Gamma Ray Observatory (GRO, NASA), the Röntgen Observatory Satellite (ROSAT, DARA/NASA/SERC), Voyager 2 (NASA), the International Ultraviolet Explorer (IUE, NASA/ESA/SERC), the Hubble Space Telescope[1] (HST, NASA/ESA), the European Southern Obser-

[1] The HST observations were obtained at the Space Telescope Science Institute, which is operated by the Association of Universities for

vatory (ESO) in Chile including the Swedish-ESO Submillimetre Telescope (SEST) and the Observatoire de Geneve facility, the Cerro Tololo Inter-American Observatory (CTIO) in Chile, the South African Astronomical Observatory (SAAO) in South Africa, the Universidad Nacional Autónoma de Méjico (UNAM), and the Very Large Array Telescope[2] (VLA) in the USA.

The data obtained in this project are presented in Sect. 2. In Sect. 3, we discuss some of the systematic differences among the various data, which arise essentially from beam size differences and thus introduce additional flux contributions which are not from the AGN itself. We outline how we have adjusted the measurements to account for these effects. We also correct all of the data for Galactic reddening, for which we have adopted a value of $E_{B-V} = 0.12 \pm 0.01$, as derived in Paper V from the fits of the HST UV spectrum presented here; this value is consistent with that inferred from the Burstein & Heiles (1982) maps, $E_{B-V} = 0.12$, and from the measured Galactic H I column density ($E_{B-V} = 0.13 \pm 0.04$, Stark et al. 1992). The pure AGN continuous emission is then derived and discussed in Sect. 4.

2. The WAD data set

In this section, we present the data, in order of increasing photon frequency, that were obtained as part of the WAD coordinated campaign. The observational parameters as well as the key points in data reduction are outlined for each observation, and the final observed flux measurements are provided.

2.1. Radio observations

The observations of NGC 3783 with the VLA began on 1992 June 27 (21:31 UT, JD 2448801.4). The phase center of the interferometer was at coordinates $\alpha_{1950} = 11^h36^m33^s$ and $\delta_{1950} = -37°27'41''$. Continuum observations were made at wavelengths of 20 cm, 3.6 cm and 2 cm with the array in the C/D hybrid configuration (Napier et al. 1983). Each observation lasted for 9 minutes. The primary flux calibrator was 3C 286 and the phase calibrator was PKS 1151−348. The observational parameters are summarized in Table 1.

The AIPS data reduction package was used to construct CLEAN images of NGC 3783, which was only partially resolved. A two-dimensional Gaussian was fitted to the image of the source at each waveband and the results are given in Table 2.

Considering the size of the synthesized beam at each waveband and the small differences between the peak and the integrated fluxes, NGC 3783 appears to be only marginally resolved at 20 cm and 3.6 cm, and unresolved at 2 cm.

Research in Astronomy, Incorporated, under NASA contract NAS5-26555.

[2] The VLA is operated by Associated Universities, Inc., a under cooperative agreement with the National Science Foundation.

Table 1. VLA parameters

	20 cm	3.6 cm	2 cm
Frequency (MHz)	1489.9	8439.9	14964.9
Bandwidth (MHz)	100	100	50
Synthesized beam (″)	41x33	7.5x6.2	3.7x3.2
3C 286 assumed flux (Jy)	14.39	5.19	3.45
PKS 1151−348 flux (Jy)	5.70	1.64	1.04
Image rms (μJy)	400	82	240

A 50 MHz bandwidth was used at 2 cm, due to calibration errors with the second IF. The assumed flux densities of 3C 286 have absolute errors of 5% (Baars et al. 1977).

Table 2. The flux measurements and properties of NGC 3783 in the radio

	20 cm	3.6 cm	2 cm
Peak flux in the beam (mJy)	32.7 (0.1)	6.07 (0.51)	2.61 (0.08)
Integrated flux 2-D gauss. (mJy)	37.9 (0.3)	8.5 (1.2)	2.49 (0.15)
Peak position (1950)	11 36 32.953 (0.008) −37 27 41.76 (0.05)	11 36 32.889 (0.004) −37 27 40.29 (0.03)	11 36 32.957 (0.011) −37 27 41.95 (0.07)
Deconvolved major axis	17″.9 (0″.4)	4″.6 (0″.1)	< 2″.3
Deconvolved minor axis	10″.9 (0″.4)	4″.0 (0″.05)	< 2″.3
Position angle	92°.2	160°	

The errors given in parentheses are the formal errors of the fit.

2.2. Far to mid-IR

No new observations of NGC 3783, due to adverse weather conditions, were obtained during the WAD campaign. For the sake of completeness, we have taken from the literature fluxes measured through N (10 μm) and Q (20 μm) filters, as well as the IRAS fluxes at 12, 25, 60, and 100 μm. We expect that most of the emission measured by IRAS (1′ to 2′ beam size) arises in cold material in the host galaxy and hence is not related with the AGN and should not vary much. Ground-based measurements in the 10 μm and 20 μm windows have been obtained through much smaller apertures (5″) by Frogel et al. (1982). These measurements are given in Table 3, despite the fact they were made at different times than the rest of the observations discussed here. Glass et al. (1982) measured a smaller broadband 10 μm flux (330±20 mJy) but through a larger aperture (7″.5) and, therefore hereafter we shall consider the Frogel et al. value.

Table 3. Far and mid-IR flux measurements from the literature

	N	Q	IRAS bands			
	10 μm	20 μm	12 μm	25 μm	60 μm	100 μm
Flux	400	1240	792	2435	3305	5118
(mJy)	±36	±250	±55	±150	±200	±560

Table 4. The near-IR fluxes, uncorrected for reddening and starlight, through a 12″ diameter diaphragm

Date (JD)	1.25 μm	1.65 μm	2.20 μm	3.40 μm
		(mJy)		
2448804	53.45	74.8	90.0	145.2
2448834	50.10	70.8	89.1	140.0
error (±)	1.40	2.0	2.5	7.0

Table 5. The ESO and CTIO spectroscopic data

Date (JD)	Aperture (″×″)	Resolution (Å)	Range (Å)	Origin
2448802.3	3×3.3	4	4750–8200	ESO
2448803.3	3×3.3	4	4750–8200	ESO
2448830.5	5×10	8	3645–7195	CTIO
2448832.5	5×10	8	3645–7195	CTIO

Comparison of the IRAS mid-IR fluxes with smaller aperture ground-based measurements provides information on the relative contributions of the AGN and host galaxy to the total flux. Using their 12 μm flux measurement through a 4″.2 aperture, Roche et al. (1991) conclude that 87% of the IRAS 12 μm flux arises from the nuclear region. For the 25 μm window, Ward et al. (1987) have extrapolated the ground-based 20 μm measurement and estimate that ~70% of the IRAS flux is due to the nucleus.

2.3. Near-IR photometry

The near IR observations were made using the 1.9m telescope at Sutherland with the MkIII photometer (Glass 1985a). The entrance diaphragm size was 12″ in diameter. A chopping procedure was used at 12.5 Hz, to fields 30″ north and south of the nucleus. The filters used are described by Glass (1973). The photometry is provided on the standard SAAO system of Carter (1990) and only J measurements needed to be transformed. The transformation of measurements on the SAAO Carter system to other systems is discussed at length by Glass (1985b). The observations were taken in exactly the same way as described by Glass (1992), who also presents the previous IR history of NGC 3783. The standard star HR 4523 was taken as a reference. Conversion to flux can be accomplished by assuming magnitude zero points of –22.82, –23.01, –23.21, –23.55 for J, H, K, L respectively, in units of log flux (watt m^{-2} Hz^{-1}). A report on the full campaign in the near IR is presented in Paper VI. From these data, we have simply taken the observations closest to the WAD primary and secondary dates on JD 2448804 and JD 2448834. These are given in Table 4. The near-IR fluxes are not corrected for reddening and include both the AGN and the stellar contributions. We shall discuss them in Sect. 3.

2.4. Optical observations

2.4.1. Direct imaging

A V band image was obtained with the CTIO 1.5m telescope at $f/7.5$ with a Tek 512x512 CCD (0″.49/pix) on 1992 June 29 (JD 2448802.5), as part of the WAD programme. The seeing, measured from unsaturated stars, is around 2″.5. The image has been calibrated by using the V measurement of NGC 3783 from Paper VI that is nearest in time to the WAD observation, which is the SAAO measurement of V = 12.92 on JD 2448803 through a 20″ diameter circular aperture. Simulated aperture photometry on the image with this aperture is used to calibrate the frame. A check of this calibration was made by performing aperture photometry through a 33″ diameter aperture and comparing the results with the OAFA measurement made on JD 2448809 (Table 3 of Paper VI). This gives V = 12.55, which is in reasonably good agreement with the OAFA value of V = 12.61. A further check is provided by comparison with the multi-aperture photometry of Schroder & Kepler (1991), obtained when NGC 3783 was about 1 mag brighter than it was on the WAD primary date (which was close to the maximum brightness during the AGN Watch campaign). By measuring the brightness of the calibrated image in the annulus defined by an aperture of diameter 15″.5 and an aperture of diameter 24″.5, we measure as the total brightness of this annular region V_{ann} = 14.43. The Schroder & Kepler data yield V_{ann} = 14.49, which is in good agreement. Given the above differences, we assume an uncertainty in the absolute flux calibration of ~6%.

2.4.2. Spectroscopy

Spectra were collected at ESO and CTIO both on and around the WAD primary and secondary dates in the course of the larger AGN Watch campaign (Paper VI). At ESO, the Boller & Chivens spectrograph attached to the Cassegrain focus of the 1.5m telescope was used, together with a CCD. At CTIO, data were obtained with the 2D-Frutti spectrometer on the 1.0m telescope. We show in Table 5 the observational parameters for spectra obtained around the WAD dates.

The data were reduced in a standard way, and all of the details can be found in Paper VI. The spectra were all put on an absolute scale by scaling the data to the [O III] λ5007 line flux, which is assumed to be constant in time as it arises in a region about 100 pc in size (i.e., ~ 0″.5 at the distance of NGC 3783, which is 38.7 Mpc for H_o= 75 km s^{-1} Mpc^{-1}). The [O III] λ5007 flux is taken to be $8.44 \pm 0.06 \times 10^{-13}$ erg s^{-1} cm^{-2}. The difference in aperture size between the two WAD spectroscopic data sets probably does not introduce more than a 2% error in the absolute scaling. The ESO spectrum obtained on JD 2448802 is displayed in Fig. 1.

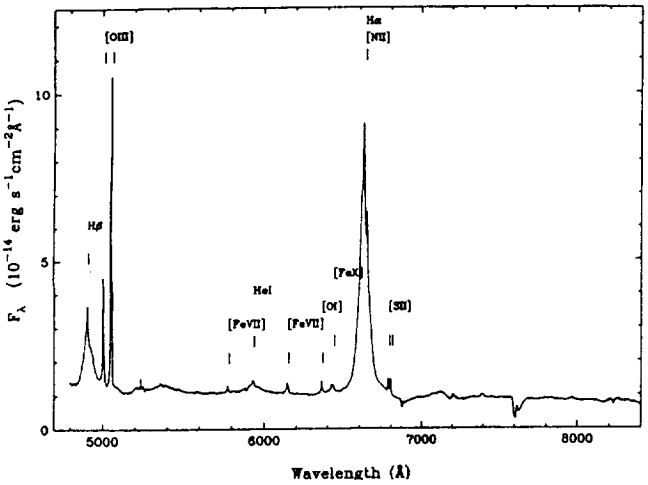

Fig. 1. Plot of the WAD long slit spectrum obtained at ESO on 1992 June 29 (JD 2448802), and extracted so as to correspond to a 3″ × 3″.3 aperture

Table 6. The optical continuum in a 20 Å bandpass centered at 5150 Å, for an entrance slit 5″ × 10″ (from Paper VI).

Date (JD)	F_λ(5150 Å) (10^{-15} erg s^{-1} cm^{-2} Å^{-1})	F_ν(5150 Å) (10^{-25} erg s^{-1} cm^{-2} Hz^{-1})
2448802.3	12.57 ± 0.62	1.11 ± 0.05
2448803.3	13.40 ± 0.64	1.18 ± 0.05
2448830.5	13.32 ± 0.27	1.18 ± 0.02
2448832.5	14.64 ± 0.29	1.29 ± 0.02

An extensive discussion on how the continuum flux was derived in a consistent manner for the whole AGN Watch campaign is provided in Paper VI. The combination of spectroscopic and photometric data led to an estimate of the continuum through a 5″ × 10″ entrance slit as given in Table 6.

Direct measurement of the ESO spectrum from 1992 June 29 (JD 2448802), again scaled by the [O III] λ5007 flux, yields a continuum measurement 10.99 ± 0.44× 10^{-15} erg s^{-1} cm^{-2} Å^{-1}. As expected, it is slightly smaller than the one derived for a 5″ × 10″ entrance slit, showing clearly that the stellar population contributes to the observed continuum. This contribution must be estimated carefully, both at visible and near IR wavelengths, to derive the pure AGN continuum emission.

2.5. *Ultraviolet observations*

2.5.1. The HST FOS data

High resolution, high signal-to-noise (S/N) ratio spectroscopic information in the ultraviolet was highly desirable in order to better understand the structure of the line-emitting regions in the AGN and to derive the Galactic reddening along the line of sight to NGC 3783. During the AGN Watch monitoring campaign with IUE (Paper V), HST observations with the Faint Object Spectrograph (FOS) were obtained for this purpose on 1992 July 27 (JD 2448830, the secondary WAD date).

Table 7. Continuum estimates from IUE spectra (10″ × 20″ entrance diaphragm), uncorrected for reddening.

JD	F_{1460}	F_{1835}	F_{2700}	F_{PL2700}	α_ν
	(10^{-14} erg s^{-1} cm^{-2} Å^{-1})				1460–1835
8801.9	4.70	4.12	3.08	2.20	1.44
	±0.13	±0.14	±0.08	±0.15	±0.03
8803.5	4.96	4.35	3.17	1.99	1.42
	±0.13	±0.11	±0.11	±0.29	±0.03
8829.3	5.47	4.85	3.70	2.57	1.47
	±0.15	±0.12	±0.12	±0.18	±0.03
8831.3	6.36	5.13	3.66	2.40	1.06
	±0.16	±0.14	±0.12	±0.23	±0.01

The nucleus of the galaxy was acquired within a 1″.0 aperture on the blue side of the FOS. We obtained a 2100 s exposure (eight separate readouts) with the G190H grating and two 1800 s exposures (each of seven separate readouts) with the G130H grating. A full description of the data processing is provided in Paper V. Over the 1160 to 2150 Å wavelength range, the line spectrum appears to be extremely rich, as discussed at length in Paper V. The absorption-line spectrum indicates a Galactic reddening $E_{B-V} = 0.12 \pm 0.01$, which was adopted as the reddening correction for NGC 3783.

Because of the HST point-spread function (PSF) at that epoch, the FOS spectrum had to be renormalized. We multiplied it by a constant factor of 1.13 to match the interpolated IUE flux at 1460 Å on the secondary WAD date. Since our current primary interest is the AGN continuous emission, we have measured the flux in the three line-free wavelength intervals of 1161–1185 Å, 1326–1330 Å, and 1340–1395 Å. The continuum flux values are listed in Table 10 below. The IUE measurements are described in next section. The difference between IUE and HST fluxes at 1328 Å and at 1368 Å, after the above normalization, is less than 5%.

2.6. *IUE spectroscopy*

The nucleus of NGC 3783 was observed with IUE throughout the International AGN Watch campaign through the large aperture (10″ × 20″) and in the low dispersion mode. Both the short wavelength (SWP, 1150–1980 Å) and the long wavelength (LWP, 1950–3300 Å) cameras were used. In particular, a number of these observations were scheduled around the WAD primary and secondary dates (Paper V). The observations on JD 2448803.5 were made especially for the WAD campaign.

All of the details concerning the processing of the IUE data can be found in Paper V. We give here the continuum measurements obtained from the Gaussian extraction (GEX) method in the windows 1445 – 1475 Å, 1820 – 1850 Å and 2680 – 2720 Å (observed wavelengths). These bandpasses were chosen from the FOS spectrum to be as free as possible of emission or absorption features. The continuum estimates are given in Table 7.

Table 7 also lists the short wavelength spectral index, α_ν ($F_\nu \propto \nu^{-\alpha_\nu}$), as measured in Paper V. It should be noted, however, that it is not corrected for reddening nor for Fe II line and Balmer continuum emission, which are important longwards of $\sim$ 1700 Å and constitute the so-called "small bump". In fact, the effective slope averaged over the whole AGN Watch campaign is estimated to change from 1.51 to 0.86 after correction for reddening in the Galaxy (Paper V) and the true index should still be flatter after correction for Fe II and Balmer continuum emission (Sect. 3).

The spectrum of the nuclear region in NGC 3783 from 1150 to 7200 Å is shown in Fig. 2. It includes the simultaneous or nearly simultaneous data collected on the secondary WAD date with HST (JD 2448830.2), with IUE (the average of the spectra obtained on JD 2448829.3 and JD 2448831.3) and at CTIO (JD 2448830.5).

2.7. *Far-UV observations*

The ultraviolet spectrometers (UVS) on board the Voyager spacecraft (Broadfoot et al. 1977) are objective grating instruments sensitive in the 500 – 1700 Å spectral range. The reciprocal dispersion is 9.26 Å per detector channel, yielding an effective resolution of about 18 Å for an unresolved source. The Voyager UVS calibration has been discussed by Holberg et al. (1982) and Holberg et al. (1991). During the observations, the Voyager scan platform is fixed in the normal direction of the target, while the spacecraft limit-cycle motions move the field-of-view (FOV) of the spectrometer on and off the target to obtain both source and background signals. In the dispersion direction, a transit of a point source through the FOV produces a well-deter:nined Gaussian-like response having an annular half-width of 0°.097. In the cross-dispersion direction, the instrument response is approximately rectangular with a full width of 0°.86.

The NGC 3783 observations discussed here were obtained with the Voyager 2 UVS during one nearly continuous observing interval between 1992 July 13 – 27, close to the secondary WAD date. For each observing interval, a continuous stream of individual spectra (500 – 1700 Å) of NGC 3783 were obtained with an integration time of 3.84 seconds. These individual spectra were combined into 15.36 second averages (3:1 compression) for logistical reasons. An aspect solution was then performed on the entire data set in order to locate NGC 3783 within the FOV. The individual spectra obtained at the nominal position of the galaxy in the FOV were accumulated, after removal of sky background, and corrected for all instrumental effects. The final ensemble spectrum, derived from the entire 14-day interval, has a total integration time of 340,425 seconds, using only data obtained within +0°.045 of the nominal position of NGC 3783 within the UVS FOV.

Because of the faintness of NGC 3783, a variety of additional data reductions were performed to evaluate external errors. The data were divided into three segments to test the confidence of detection; this yielded certain detection in 2 segments, probable detection in the third. Reductions using local and non-local background were performed, producing spectra with no statistically significant differences. The effect of uncertainties in the aspect solution was evaluated by comparing spectra summed on different centers (Center 1 and Center 2) in the Voyager FOV. These external error evaluations were combined with the internal (photon) errors of the final ensemble spectrum for analysis.

Table 8. Broad-band average far-ultraviolet flux through the 0°.1 × 0°.8 Voyager FOV entrance

	F_λ (erg cm^{-2}s^{-1}Å^{-1})	
Bandpass	925 – 1000 Å	1045 – 1120 Å
Center 1	1.83×10^{-13}	4.71×10^{-13}
Center 2	1.63×10^{-13}	4.64×10^{-13}
Adopted value	1.7×10^{-13}	4.7×10^{-13}

Uncertainties are 8×10^{-14} erg s^{-1} cm^{-2} Å^{-1}.

The faintness of NGC 3783 precludes use of data in the lower sensitivity, longer Voyager wavelengths (1150–1700 Å). For the shorter wavelength Voyager data, the per-channel errors were still significant and it was decided to bin the data into 2 broad bands to improve the S/N ratio. The results for this two bins are shown in Table 8, along with estimates of the total (internal plus external) error. The 963 Å flux has been corrected for reddening by the interstellar medium, by extrapolating the Seaton's law (1979) using the extinction at 1010 and 1000 Å. We shall discuss in Sect. 3 the association of this flux measurements with the AGN in NGC 3783.

2.8. *Soft X-ray observations*

As part of the WAD project, NGC 3783 was scheduled as a target of opportunity for two orbits of the ROSAT X-ray telescope (Trümper 1993) with the Position Sensitive Proportional Counter (PSPC-B) in the focal plane (Pfeffermann et al. 1986). The PSPC is sensitive over the bandpass 0.1 – 2.4 keV, and has a 2° diameter FOV. The spatial resolution (FWHM) for the full bandpass is around 25″ on axis and 44″ at an off-axis angle of 11′ (Hasinger et al. 1992). The energy resolution (FWHM) of the PSPC detector is $\Delta E/E = 0.43(E/0.93)^{-0.5}$, where E is the photon energy in keV.

Due to operational problems with the satellite, only one short observation could be performed on 1992 July 1 (from UT 20:42:10 to 21:03:27), with an effective on-source integration time of 402 seconds. The average count-rate on the source, i.e., corrected for background, was 2.22 ± 0.08 s^{-1}, which enables us to perform only a limited spectral fitting. A simple power law fit to the photon-energy distribution $N(E) \propto E^{-\Gamma}$ yields a photon index $\Gamma = 2.56 \pm 0.39$, assuming a Galactic absorption $N_H = 9.4 \times 10^{20}$ cm^{-2} (Stark et al. 1992), consistent with the E_{B-V} value discussed in Sect. 1. This fit results in an unabsorbed X-ray flux of $1.03 \pm 0.3 \times 10^{-10}$ erg s^{-1} cm^{-2} over the 0.1 – 2.4 keV window. However, the reduced χ^2 indicates that

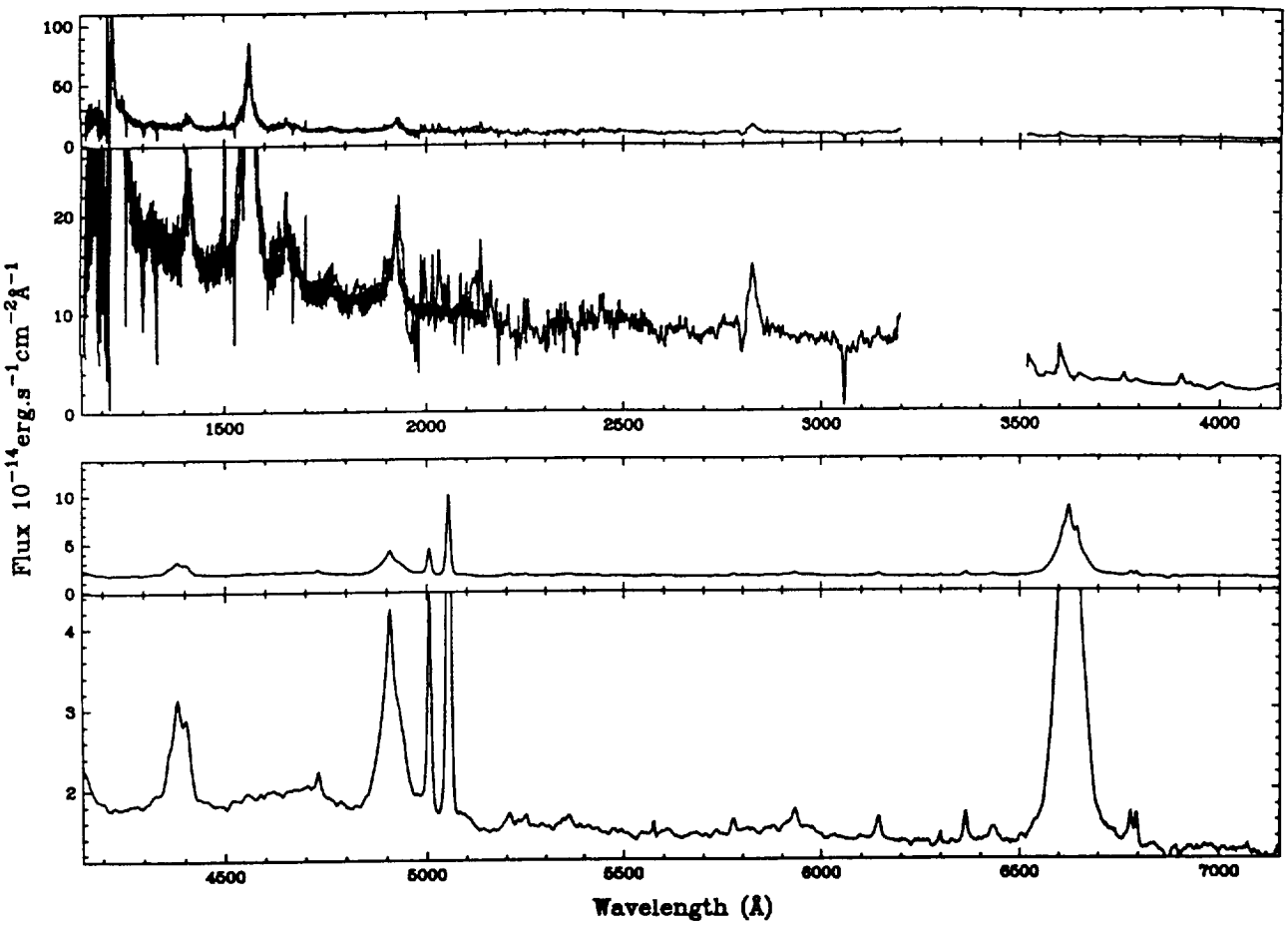

Fig. 2. Plot of the nuclear spectrum of NGC 3783 obtained on the secondary WAD date by HST, IUE and the CTIO 1m telescope through apertures of 1″, 10″ × 20″ and 5″ × 10″ respectively. The spectrum has been corrected for reddening in the Galaxy, but not for the host-galaxy starlight contribution, which is nearly negligible in the UV but important and aperture-dependent at optical wavelengths. Different scales are used to show both weak and strong features, in particular, the scales in the bottom panel are enhanced by a factor of 8

the fit is not acceptable. Indeed, a more complex fit is required, as an absorption structure around 1 keV indicates the presence of a warm absorber.

Fortunately, another observation of NGC 3783 with the PSPC aboard ROSAT was scheduled on 1992 July 23, falling in the window of the secondary WAD date (Turner et al. 1993). The total on-source exposure time was 2668 sec. The data reduction procedure is described in detail by Turner et al. (1993). The larger number of counts obtained in this second exposure allows a spatial analysis to be performed. The X-ray emission is found to be point-like at the resolution of the instrument. Turner et al. report an averaged 0.1 – 2.0 keV count-rate of $1.10 \pm 0.02\,s^{-1}$ and obtain an unabsorbed integrated flux of 4.9×10^{-11} erg s^{-1} cm^{-2} after a simple power law fit in the 0.1 – 2.0 keV range, using values for the best fitting parameters which are only slightly different from that shown above (i.e. $\Gamma = 2.46$ and an assumed Galactic absorption of $N_H = 8.7 \times 10^{20}\,cm^{-2}$, or $E_{B-V} = 0.12$). This indicates that the soft X-ray flux decreased by roughly a factor of two from the 1^{st} to the 23^{rd} of July, 1992. Although there is some evidence for flux variability on a time scale of 10 hours, no change is noticeable in the 0.1 – 2.0 keV X-ray spectral shape. We shall adopt hereafter the fit of the mean spectrum and flux level obtained on 1992 July 23.

Two types of fitting have been applied to the PSPC data, (i) a simple power law fit, which as already mentioned is found to be unsatisfactory, (ii) a power law plus absorption edge, which following the models by Yaqoob & Warwick (1991) and Netzer (1993) arises in highly ionized material (carbon and oxygen) in the immediate vicinity of the AGN continuum source. This model provides by far the better fit and therefore we have used for the secondary WAD date the results from Turner et al. (1993), with the photon index Γ fixed at a value of 1.9. The inferred column density of absorbing cold material along the line of sight is $N_H = 1.08 \pm 0.1 \times 10^{21}\,cm^{-2}$, again consistent with the FOS determination (Paper V and Sect. 1). The best fit to the warm absorber model yields $N_H^{ion} = 156^{+23}_{-47} \times 10^{21}\,cm^{-2}$. The total X-ray continuum flux (uncorrected for Galactic absorption) for this model is 1.6×10^{-11} erg s^{-1} cm^{-2} in the 0.1 – 2.0 keV band. The continuum fluxes at 0.1, 1.0, and 2.5 keV are given in Table 10. Note that for the WAD primary date, we have taken

the WAD secondary date measurements multiplied by a factor of 2, following the count-rate comparison at the two dates.

As discussed by Turner et al. (1993), the final fit is quite consistent with previous X-ray results for NGC 3783 from *Ginga* and EXOSAT; both of these satellites were also sensitive to higher-energy X-rays, and in fact the 2 – 10 keV spectrum of NGC 3783 is well fitted by a single power law with the same spectral index as the 0.1 – 2.5 keV spectrum ($\Gamma = 1.9$) plus the signatures of the highly ionized warm absorber in the form of absorption edges. We can therefore with some confidence extrapolate the fit to the ROSAT data up to at least 10 keV.

2.9. *Gamma-ray observations*

The Compton Gamma Ray Observatory (GRO) spacecraft (Gehrels et al. 1993) observed NGC 3783 from 1992 June 25 through 1992 July 2. Marginally significant flux was detected in the 0.05 – 0.15 MeV band by the Oriented Scintillation Spectrometer Experiment (OSSE), which covers the energy range from 0.05 to 10 MeV (Johnson et al. 1993). No significant flux from NGC 3783 was detected by OSSE at energies above 0.15 MeV (cf. Table 9).

The OSSE field of view is approximately $4° \times 11°$, and non-source background flux is estimated by viewing 4°.5 to either side of the source field during the observation. The $4° \times 11°$ field does allow the possibility of source confusion; however, based on historical data there are no more probable candidates in the source field than the AGN in NGC 3783 and in this paper we will assume that only NGC 3783 is contributing to source flux in the OSSE field.

A search for high-energy γ-ray emission from NGC 3783 with data from the EGRET all-sky survey has been unsuccessful (Lin et al. 1993). The EGRET telescope, which is also on board the GRO satellite, is sensitive to photons in the energy range 20 MeV – 30 GeV. For data obtained on 1991 October 17 and 31, Lin et al. (1993) find a 2σ upper limit for the NGC 3783 photon flux at $E > 100$ MeV of 1.2×10^{-7} photons cm^{-2} s^{-1}, which is just at the detection threshold of the instrument (1.0×10^{-7} photons cm^{-2} s^{-1}). The situation is similar for all the Seyfert 1 galaxies studied by Lin et al. (a total of 22, most of them strong X-ray emitters). In their work, Lin et al. suggest that a spectral break from the hard X-rays to the γ-rays may be a common feature in the energy distribution of such objects.

Table 9. Gamma-ray fluxes from OSSE

Energy (MeV)	Photon flux (10^{-3} ph. cm^{-2} s^{-1} MeV^{-1})	Comments
0.05 – 0.15	3.1 ± 1.1	
0.15 – 0.50	< 0.8	2σ upper limit
0.50 – 1.00	< 0.9	2σ upper limit

3. Isolation of the "pure" AGN continuum: systematic corrections to the data

The continuum emission that is generally associated directly with the AGN phenomenon (the "pure" AGN continuum) is thought to arise in various physical components that range in size from $\sim 10^{13}$ to $\sim 10^{18}$ cm. The size estimates, which are generally based on variability arguments, can be understood within the general framework of the black hole and accretion-disc model for AGN. From an observational point of view, we expect therefore the AGN continuum to arise at all wavelengths from a point-like source.

The various instruments and techniques used in this multi-wavelength program employ different effective beam sizes in the different wavebands. This introduces two difficulties. First, when the field of view of the instrument is larger than the size of NGC 3783, we shall have to establish that no other source contributes to the observed flux (for example, in the ROSAT and Voyager data). Second, even if the field of view is small enough that there is no ambiguity in the source identification, it must be remembered that the AGN itself is embedded in larger components, such as the stellar population in the bulge of its host galaxy: we must carefully estimate the flux in such components in order to isolated the "pure" or uncontaminated AGN spectrum, which we present in Table 10 and Fig. 3.

3.1. *Radio emission*

The radio flux at 20 cm probably includes some continuous emission from the galactic disc in NGC 3783. At 3.6 cm the observed source is only marginally resolved, while at 2 cm it is still unresolved. Taking into account the beam sizes and comparing the peak and integrated fluxes (Table 2), we conclude that 80% of the 3.6 cm flux and 100% of the 2 cm flux are attributable to AGN activity. These values are given in Table 10.

3.2. *Far IR to mid-IR emission*

Following Roche et al. (1991) and Ward et al. (1987), we can estimate the fraction of the far and mid-IR fluxes directly attributable to the AGN in NGC 3783. Again, these values are given in Table 10, although they are not contemporaneous with the WAD data set. This spectral component probably arises from cool dust close to the central continuum source, but occupying a far more extended region. It is a matter of debate as to whether or not the dust component should be considered a genuine part of the AGN, and we will return to this point in Sect. 4.

3.3. *The near-IR emission*

The near-IR emission may arise from three sources, (i) the stellar population surrounding the AGN, (ii) hot dust close to the AGN, at about 80 light-days from the centre (Glass 1992), and (iii) the AGN continuous emission source. We shall consider that components (ii) and (iii) are both part of the AGN, and we shall apply a correction for the contribution from the stellar population only.

The stellar contribution in the near IR has been estimated by Glass (1992), assuming that the stellar population in the central region of NGC 3783 exhibits infrared colours similar to that of

a normal galaxy. His procedure yields a galactic flux (before correcting for reddening) of 27.9 ± 0.7, 37.0 ± 0.6, 29.2 ± 0.4, and 16.3 ± 0.4 mJy in the J, H, K, and L bands, respectively. By subtracting this contribution, we obtain the fluxes given in Table 10.

3.4. The optical continuum

In low-luminosity AGNs, such as NGC 3783, separation of the stellar and non-stellar contributions to the optical spectral energy distribution takes on particular importance because the surface brightness distribution of the stellar contribution is far more extended than that of the point-like AGN. Thus, the relative contribution of each component to the observed optical spectrum is a function of both spectrograph entrance aperture geometry and seeing, and the surface brightness distribution needs to be known to compare data obtained with different instruments and under different observing conditions. We have attempted two different types of analysis to estimate the starlight contamination of the optical spectra obtained as part of this programme, and these are described below.

3.4.1. Spectroscopic estimate of the stellar contribution

One method of measuring the starlight contribution to an AGN spectrum is by determining the dilution of the stellar absorption features by the featureless AGN continuum. The weakness of this method is that one must know a priori the undiluted equivalent widths of the galaxian absorption features. We have constructed a template galaxian spectrum from the off-nuclear CCD spectra, and have scaled this spectrum in flux by trial-and-error until the absorption features vanish in the difference spectrum obtained by subtracting the scaled extranuclear spectrum from the nuclear spectrum. The implicit assumption in this method is that the starlight spectrum does not change drastically with distance from the centre of the galaxy. The extranuclear spectrum was constructed from the long-slit CCD spectra obtained with the ESO 1.5m telescope. One of these spectra, which covers the spectral range 4750 – 8200 Å, was obtained as part of this program (Table 5), and another was collected as part of the NGC 3783 monitoring campaign (Paper VI). The latter spectrum, obtained on 1991 December 19, covers the useful spectral range 3700 – 7000 Å. An extranuclear spectrum was constructed from each of these two-dimensional images by extracting separately two one-dimensional spectra, the first one centered on the nucleus and extending 5″.3 in either direction, and the second also centered on the nucleus and extending 9″.9 in either direction. The difference spectrum produced by subtracting the 5″.3-wide spectrum from the 9″.9-wide spectrum gives the host galaxy spectrum (or at least its bulge spectrum) in the range 5″.5 to 9″.9 (1 to 1.9 kpc for $H_o = 75$ km s^{-1} Mpc^{-1}) from the nucleus. These limits were chosen to maximize the S/N ratio of the difference spectrum and to remove all of the scattered broad-line features to better than 1%. Several trials revealed that smaller inner limits left residual broad-line features in the difference spectrum. Since the AGN continuum and the broad-line emission both arise on scales that are effectively point-like, the absence of scattered broad lines in the final spectrum also suggests that the difference spectrum is free of scattered AGN continuum emission to better than 1%. Similarly, the outer limit was chosen as a result of several trials in order to achieve the maximum S/N ratio in the difference spectra.

The difference spectra from the two separate epochs match extremely well over the region of overlap, and were thus merged to form a final starlight template.

The starlight contribution to the nuclear spectra was estimated by comparing the equivalent widths of stellar absorption features, principally the Mg I and MgH b lines in the range 5156 – 5196 Å in the nuclear spectrum to those in the extranuclear spectrum. The difference spectra obtained by subtracting the scaled extranuclear spectrum from the nuclear spectrum were also examined carefully to reduce the chances of being misled by the effects of weak emission lines (such as broad Fe II features) in the nuclear spectra.

On the basis of this analysis, we conclude that the starlight contribution to the ESO 3″ × 3″.3 nuclear spectra is less than 20%, and that the starlight contribution in the CTIO 5″ × 10″ nuclear spectra is less than 30%. The latter number in particular is not very well determined because of the limited S/N ratio of the data, so we repeated the analysis after forming a higher S/N average spectrum by combining all of the CTIO spectra collected during the eight-month NGC 3783 monitoring campaign (Paper VI). The measured continuum level of this average spectrum at 5150 Å differs from the continuum level of the spectrum obtained near the primary WAD date by only a few percent. The estimated starlight contribution to this average spectrum is also estimated to be about 30%.

3.4.2. Direct imaging estimate of the stellar contribution

Direct V band imaging of the NGC 3783 field can be used to obtain a completely independent estimate of the starlight contamination of the optical spectra. In this method, we model the surface brightness distribution of NGC 3783 as the sum of an extended galaxian component plus a central unresolved source which represents the active nucleus. The observed surface brightness distribution of the nucleus alone is thus assumed to be given by the PSF, which can be readily obtained from stellar images in the same frame.

Separation of the observed surface brightness distribution was accomplished by modeling the AGN component with the observed PSF and the starlight component with plausible seeing-convolved galaxian surface brightness distributions such as a de Vaucouleurs $r^{1/4}$ law and an exponential disc. This analysis was complicated only slightly by the fact that NGC 3783 has a barred structure. This analysis turns out to be quite insensitive to the adopted form of the galaxian surface brightness distribution, and the relative fluxes in the two components are repeatable to within a few percent.

Once the relative fluxes in the two components have been determined, the relative contribution of the star light in V through an arbitrary spectrograph aperture can be estimated by compar-

ing the results of simulated aperture photometry for the original image and the AGN-subtracted image. The analysis indicates that the starlight contribution to the ESO spectrum ($3'' \times 3''.3$) is 16%, and the contribution to the CTIO spectrum ($5'' \times 10''$) is 29%. These results depend somewhat on the seeing: as the seeing worsens, relatively more light is lost from the more concentrated components. The magnitude of this effect can be estimated by convolving the images with Gaussians to obtain a broader PSF. The CTIO aperture is large enough to be fairly insensitive to seeing effects, and the observed starlight fraction increases only to 32% for seeing as poor as 5″ (FWHM). In contrast, the starlight contribution to the ESO spectrum depends more critically on the seeing because of the smaller aperture. For the ESO aperture, the starlight fraction increases to 20% for 4″ seeing and to 24% for 5″ seeing. The actual seeing conditions under which the ESO spectrum was obtained can be estimated from the original two-dimensional spectrum by making use of the fact that the cross-dispersion profile of a long-slit spectrum is the monochromatic surface-brightness distribution (Baribaud et al. 1994). We extracted two cross-dispersion cuts from the two-dimensional spectrum, one through the wing of the broad Hβ feature and one at an adjacent continuum wavelength. Subtraction of the continuum cut from the Hβ cut yields the surface brightness distribution of the broad Hβ line, which is the PSF since the BLR is spatially unresolved. From this analysis, we estimate that the seeing for the ESO spectrum is about 2″.6. Simulated aperture photometry on the appropriate convolved V image indicates that the starlight contribution to the observed spectrum should be around 16%, which is consistent with the spectroscopic estimate. We have also investigated the possible effects of miscentering by repeating the imaging analysis with the simulated aperture centers displaced from the nominal image center by up to 1″ to the south and 1″ to the west. This was found to have a very small impact and thus is not considered further.

The stellar contribution to the optical emission at 5150 Å corresponds to $4.5 \pm 0.4 \times 10^{-15}$ erg s^{-1} cm^{-2} Å^{-1} within the CTIO 5″ × 10″ aperture and $1.5 \pm 0.2 \times 10^{-15}$ erg s^{-1} cm^{-2} Å^{-1} within the ESO 3″ × 3″.3 aperture. These numbers are respectively 29% and 16% of the measured flux through the corresponding apertures. Using 29% and 16% of the 5150 Å flux in the spectra we would obtain 3.8 ± 0.3 and $1.8 \pm 0.1 \times 10^{-15}$ erg s^{-1} cm^{-2} Å^{-1} respectively. We consider hereafter the mean values of 4.2 ± 0.7 and $1.7 \pm 0.3 \times 10^{-15}$ erg s^{-1} cm^{-2} Å^{-1}. These estimates yield for the nuclear flux at 5150 Å on the primary WAD date values of 9.3 ± 0.5 and $8.8 \pm 1.0 \times 10^{-15}$ erg s^{-1} cm^{-2} Å^{-1}, as measured in the ESO spectrum and with the aperture photometry of Table 6, respectively. They are fully consistent and hence we use their average value.

The above quantities can be compared to previous estimates. Kotilainen et al. (1993) have performed a surface brightness profile decomposition in NGC 3783, which is similar to our method but based on independent CCD images. Using their fit in the optical (V band) and an entrance circular aperture of 1″.775 radius to simulate the ESO 3″ × 3″.3 aperture, we derive a stellar flux contribution of 2.25×10^{-15} erg s^{-1} cm^{-2} Å^{-1}. The difference between this estimate and ours is probably due to both absolute calibration uncertainties and seeing losses (which are not taken into account in this computation). Winkler et al. (1992) estimate the host galaxy flux through circular 20″ and 30″ diameter apertures to be 1.54×10^{-14} erg s^{-1} cm^{-2} Å^{-1} and 2.27×10^{-14} erg s^{-1} cm^{-2} Å^{-1}, in reasonable agreement with the values obtained by simulated aperture photometry with our V image, i.e. 1.34×10^{-14} erg s^{-1} cm^{-2} Å^{-1} and 2.06×10^{-14} erg s^{-1} cm^{-2} Å^{-1}.

We can also compare these figures with the amount of light from the underlying galaxy within three different apertures (18″, 20″, and 33″) as inferred by Stirpe et al. (Paper VI) in a completely independent way. In that paper, the positive offset in the linear correlation of pairs of quasi-simultaneous fluxes from photometric and CTIO spectroscopic data-sets is interpreted as caused by the underlying galaxy's higher contribution through the larger apertures. Adding the galaxy flux that contaminates the spectra to the mean offsets, we obtain the stellar flux through the photometric aperture. This method yields 1.312 ± 0.084, 1.421 ± 0.077 and $2.114 \pm 0.065 \times 10^{-14}$ erg s^{-1} cm^{-2} Å^{-1} for the three apertures. Measuring the same quantity in the deconvolved V frame we get (quoting the 6% of uncertainty in the absolute flux scale): 1.239 ± 0.074, 1.343 ± 0.081, and $2.34 \pm 0.14 \times 10^{-14}$ erg s^{-1} cm^{-2} Å^{-1}, in fairly good agreement with the above results.

The galaxian V flux through the 12″ aperture used in the near IR observations, as measured in our CCD image, is 8.15 mJy (8.09×10^{-15} erg s^{-1} cm^{-2} Å^{-1}). This, together with the results from the previous subsection, gives an V–K color for the underlying galaxy of 3.3 ± 0.2 or 3.0 ± 0.3 after reddening correction, compatible with the "standard" value for normal galaxies of 3.22 ± 0.10 (Glass 1984).

3.5. Ultraviolet emission

3.5.1. The "small bump" contribution

The 2680 – 2720 Å window is quite sensitive to the Fe II and Balmer continuum contributions, which together comprise a strong emission blend known as the "small bump." In Paper V, the 2000 – 3000 Å spectral range was modeled with a synthetic blend of Fe II emission lines and an underlying power law continuum which is normalized by the values of F_{PL2700} given in Table 7. This model does not, however, include a contribution from the Balmer continuum, and we have therefore considered whether or not this leads to a significant overestimate of the continuum flux at 2700 Å. We have compared the results shown here with a fit to a mean UV-optical spectrum of the nucleus in NGC 3783, averaged over a ~10-year period (using the IUE observations of NGC 3783 obtained between 1978 and 1985 and a number of optical spectra obtained at ESO during the same period, though not simultaneously). The procedure followed is similar to that described in Wamsteker et al. (1990), and employs synthetic spectra from Wills et al. (1985). In the time-averaged spectrum, the Fe II and Balmer continuum con-

tributed together ~35% of the total 2700 Å flux (Santos-Lleó & Alloin 1995). The results of the "small bump" decomposition of Paper V, shown in Table 7, suggest that the Fe II contributes ~33% to the observed flux at 2700 Å. These two values are in rather close agreement, and although the relative contributions of Fe II and Balmer are unclear, consistent results for the relative strength of the underlying power law are obtained. We shall therefore assume that the values of F_{PL2700} in Table 7 are indeed reasonably good estimates of the nuclear continuum emission. The 1835 Å window contains also a contribution from the "small bump" which has been estimated to be ~9% of the observed flux F_{1835} (Santos-Lleó & Alloin 1995). A constant contribution of 0.99 mJy (after correction for reddening) has therefore been subtracted from the values reported in Table 7 to account for "small bump" contamination of the 1835 Å window.

3.5.2. Estimate of the UV stellar contribution

The $10'' \times 20''$ entrance aperture of the IUE instruments projects to a 2 kpc × 4 kpc region at the centre of NGC 3783 ($H_o = 75\,km\,s^{-1}\,Mpc^{-1}$). Therefore, the IUE flux may include some stellar contribution from the bulge of the galaxy.

The galaxy is of an SBa type, corresponding to group S1 in Bica's (1988) analysis of the stellar populations in the central regions of normal galaxies. In group S1, the fit of the stellar composite spectrum from 3700 to 10000 Å indicates that there is no population with an age less than 10^9 years. Hence, there should be no flux contribution over the IUE wavelength region from the bulge stellar population of NGC 3783.

However, the bulge population of NGC 3783 might be different from that of a normal galaxy with the same galaxy type if, for example, recent star forming activity has been taking place close to the AGN. In such a case, we would expect to see signs of this activity in the long-slit spectroscopic data obtained at ESO or in the V band image obtained at CTIO (Sect 2.4). However, these data show no evidence for recent nuclear star formation, and we therefore conclude that there is likely no contribution from a very young stellar component in the ultraviolet data.

There is also the possibility that the bulge stellar population has a UV turn-up, as in the nuclear stellar population of some elliptical galaxies, regardless of whether it might be an age or metallicity effect. As discussed, for example, by Bica & Alloin (1988), the UV flux of such a population could be as large as $F_\lambda(1500Å) \approx 0.25F_\lambda(5870Å)$. As we discussed above, the stellar contribution at ~ 5150 Å to the CTIO data ($5'' \times 10''$ entrance aperture) is less than 30% of the total, or about $4.5 \pm 0.4 \times 10^{-15}\,erg\,s^{-1}\,cm^{-2}\,Å^{-1}$. With the ultraviolet-to-visible flux ratio given above, this would result in a contribution in the ultraviolet less than $1.12 \pm 0.1 \times 10^{-15}\,erg\,s^{-1}\,cm^{-2}\,Å^{-1}$ at 1460 Å. The IUE entrance diaphragm is indeed larger ($10'' \times 20''$) than that used in the CTIO observations, but the UV turn-up has been detected only in the central regions of elliptical galaxies. There is no strong support for a UV turn-up in the extranuclear regions. In conclusion, we estimate that a possible UV turn-up would not contribute more than 2% of the measured IUE flux.

Finally, another estimate of the possible ultraviolet contribution from the stellar population in NGC 3783 was performed by scaling an IUE plus ground-based spectrum of M 32 to the optical spectrum of Bica's (1988) group S1 (Santos-Lleó & Alloin 1995). Again, we find that the stellar contribution is negligible (< 0.5% at 2700 Å) in the IUE NGC 3783 spectra.

3.6. Far ultraviolet emission

The FOV of the Voyager instrument is rather large ($0^\circ.1 \times 0^\circ.8$) and, in addition, the orientation of this aperture on the sky changes during the observation. However, the NGC 3783 spectrum we use was extracted when the target was near the centre of the FOV, with a slit position angle around 45°.

We have carefully searched for other likely contributors to the ultraviolet flux in the FOV, either reddened O stars with a V magnitude less than 10.9 or white dwarfs with a V magnitude less than 16. From the catalogue of O stars by Klare & Szeidl (1966), we find no possible contributor in the FOV. This is not surprising as NGC 3783 is at Galactic latitude 23°, high above the Galactic plane. We have also searched for possible white dwarfs in this FOV by examining the catalogues of Luyten (1977), which is complete to 19 mag, and of Agayev et al. (1982), which is complete to 17 mag. In neither of these do we find possible white dwarfs that might contaminate the NGC 3783 Voyager flux measurement. There is however a stellar source fairly close to NGC 3783, it is the star HD 101274 ($\alpha_{2000} = 11^h39^m06^s$ and $\delta_{2000} = -37°45'13''$, note that for NGC 3783 $\alpha_{2000} = 11^h39^m02^s$ and $\delta_{1950} = -37°44'18''$). It is an A0V type star with magnitudes m_V=9.3 and m_B=9.3. In principle, neither far UV nor X-ray emission is expected from such type of stars. In addition, a search was made in the ROSAT wide field camera survey for sources in the Voyager error box. The nearest one found is 7° away from the error box centre. Thus, we find no obvious contaminating source in the field.

3.7. Soft X-ray emission

The spatial resolution of the PCSP experiment is sufficiently small, 25″ on axis, that there is no uncertainty in the source identification. We disregard the possible occurrence of stellar X-ray contributors in the vicinity of the nucleus of NGC 3783 since such sources are likely to be intrinsically much fainter than the AGN itself.

4. Discussion and concluding remarks

4.1. The "pure" AGN spectral energy distribution

The "pure" AGN spectral energy distribution in NGC 3783 is shown in Fig. 3, based on the corrected fluxes given in Table 10. This figure comprises data obtained during both the primary and secondary WAD dates — one month apart — and previously published measurements of the far IR. From the IUE monitoring program (Paper V), we know that the UV flux on the secondary WAD date was ~20% higher than on the primary date. In the context of the broad wavelength coverage of the

WAD campaign, this constitutes a small variation which does not change considerably the interpretation of the overall energy distribution.

In the UV, we observe a surprisingly large flux increase between 1460 Å (from IUE) and 1100 Å (from Voyager 2). The IUE points in Fig. 3 represent the observed fluxes on the primary and secondary WAD dates, while the Voyager estimate corresponds to a continuous integration of 14 days (1992 July 13 – 27). The mean 1460 Å IUE flux, sampled every 2 days in the IUE monitoring program (Paper V), over the time of the Voyager integration is $5.2 \pm 0.3 \times 10^{-14}$ erg s^{-1} cm^{-2} Å^{-1} ($1.30 \pm 0.08 \times 10^{-13}$ erg s^{-1} cm^{-2} Å^{-1} after correcting for Galactic absorption); the 1083 Å Voyager flux reported in Table 8, corrected for Galactic absorption, is $1.8 \pm 0.3 \times 10^{-12}$ erg s^{-1} cm^{-2} Å^{-1}, still a factor 14 ± 3 larger than the IUE 1460 Å flux.

Is it possible that the large difference between the IUE and Voyager fluxes is real and attributable to source variability? One possible explanation that we regard as very unlikely given the past variability history of NGC 3783 (e.g. Paper V and references cited therein) is that a few very intense and brief (less than 2 days) continuum outbursts occurred in between consecutive NGC 3783 IUE observations and therefore not detected by IUE but nevertheless accumulated in the Voyager integrated spectrum. Another possibility is that the 1083 Å continuum is varying out of phase with the 1460 Å continuum, but this is exceedingly unlikely as we surely would have seen the signature of such an occurrence in the IUE spectra, which can be traced accurately to wavelengths as short as $\sim$ 1150 Å.

The absolute calibrations for both experiments have been checked carefully with flux standards. A Voyager UVS flux calibration problem for very faint objects can also be excluded as observations of faint white dwarfs and cataclysmic variables show no evidence for such an effect; the Voyager calibration matches that of IUE down to the detection limit of the instrument.

We have already excluded obvious contamination by foreground objects to the large-aperture Voyager data (Sect. 3.6). However, the possibilities of either an unknown companion to a brighter star or a spectral misclassification of an O or a B star to late-B still remain. Also, there have been rare instances in the past when an unusual reflection off the walls of the UVS instrument mimics a faint star, but usually these events are much shorter than 14 days. Given the lack of viability of the various possibilities that we have considered, the most likely explanation for the discrepancy between the IUE and Voyager results is that there is an unknown source in the much larger field-of-view of the Voyager instrument that greatly dominates the flux from NGC 3783 in the far-UV band.

4.2. The AGN related components

Although we do not yet have a clear picture of the interrelation between all the processes at work in an AGN, we know that the physics must be quite complicated. It is not even obvious what physical components are genuinely associated with the AGN itself or how they will manifest themselves in the spectral energy distribution. A complete and consistent description of the AGN phenomenon remains to be worked out. In the following, we shall consider the family of AGN models involving a central massive black hole surrounded by an accretion disc.

In addition to emission that is directly attributable to the accretion process, we also identify as "related components" induced effects such as heated dust in the vicinity of the AGN (whose obvious spectral signature is discussed in Sect. 4.3.2) and X-ray heated winds, which might also produce absorption features in the AGN spectrum. Under appropriate physical conditions, the warm absorber necessary to match the ROSAT soft X-ray spectrum of NGC 3783 can be plausibly associated with the UV absorption lines visible in the FOS spectrum. The blue shifts of the lines suggest outflow velocities of 600 to 700 km s^{-1}, comparable to the X-ray heated wind in NGC 1068 (Krolik & Begelman 1986). A similar wind may be the source of the warm absorbing material in NGC 3783. For the specific model discussed by Turner et al. (1993) ($T = 10^5$ K, $N_H^{ion} = 1.56 \times 10^{23}$ cm^{-2}, and log U = 1.45), column densities for H I and C IV are predicted to be 1.3×10^{16} cm^{-2} and 8.4×10^{11} cm^{-2}, respectively. This is sufficient to produce the 0.8 Å equivalent width Lyα line, but it cannot account for the comparably strong C IV feature. However, if the wind starts out hotter and more highly ionized, the outer portions of the wind may achieve more commensurate columns in hydrogen and lower ionization species such as C IV as it cools. Testing this hypothesis will require more complete modeling of the warm absorber.

4.3. Decomposition of the overall energy distribution

Above radio frequencies, the spectral energy distribution of the AGN in NGC 3783 is nearly flat in the $\log \nu F_\nu$ vs. $\log \nu$ plane, as is typical of radio-quiet AGNs. In the high-energy domain, the 0.1 MeV flux is approximately what would be expected from simple extrapolation of the X-rays. Unfortunately, the 2σ upper limits on the more energetic γ-ray fluxes do not allow further constraints to be set. In particular, it is still uncertain whether or not the flat spectral energy distribution breaks down for energies above $\sim$ 0.1 MeV. In the absence of any meaningful constraints, we will proceed with this discussion assuming a high-energy (0.1 MeV to 0.1 keV) photon distribution which is characterized by a power law $F_\nu \propto \nu^{-\alpha}$ of index $\alpha \approx 1$. We note that even the 100 MeV flux upper limit ($\sim 8 \times 10^{-6}$ mJy, Sect. 2.9) lies above the extrapolation of the $\alpha = 1$ power law at this energy ($\sim 2 \times 10^{-7}$ mJy). We also note in passing that the OSSE composite Seyfert spectrum created from the sum of 26 observations of 15 of the weaker γ-ray detected Seyferts indicates a mean γ-ray spectrum that is softer than that seen in the X-rays. The best fit to it is obtained by simple exponential with e-folding energy of 46 keV, which is consistent with no detection of any Seyfert nuclei at higher γ-ray frequencies (Johnson et al. 1994).

In attempting to fit the observed spectral energy distribution over a broader wavelength range (from γ-ray to infrared wavelengths), we consider two distinct spectral decompositions. In

Table 10. The "pure" AGN spectral energy distribution of NGC 3783

Frequency (Hz)	λ or Energy	Primary Date F_ν(obs) (mJy)	Primary Date F_ν(cor)[a] (mJy)	Secondary Date F_ν(obs) (mJy)	Secondary Date F_ν(cor)[a] (mJy)	Comments
$1.50\,10^9$	20 cm	37.9 ± 0.3[b]		...	...	Size 18″ × 11″, partially resolved
$8.44\,10^9$	3.6 cm	6.8 ± 1.0		...	...	
$1.50\,10^9$	2 cm	2.49 ± 0.15		...	...	
$1.20\,10^{13}$	25 μm		1740 ± 100			5″, Ward et al. 1987
$1.50\,10^{13}$	20 μm		1240 ± 250			5″, Frogel et al. 1982
$2.50\,10^{13}$	12 μm		689 ± 40			4″.2, Roche et al. 1991
$3.00\,10^{13}$	10 μm		400 ± 36			5″, Frogel et al. 1982
$8.82\,10^{13}$	3.4 μm	129 ± 7	130 ± 7	124 ± 7	125 ± 7	
$1.36\,10^{14}$	2.2 μm	61 ± 3	63 ± 3	60 ± 3	62 ± 3	
$1.82\,10^{14}$	1.65 μm	39 ± 3	41 ± 3	35 ± 3	37 ± 3	
$2.40\,10^{14}$	1.25 μm	26 ± 2	29 ± 2	23 ± 2	25 ± 2	
$5.83\,10^{14}$	5150 Å	8.0 ± 1.0	11.7 ± 1	8.6 ± 1	12.7 ± 1	
$1.11\,10^{15}$	2700 Å[c]	7.58 ± 0.46	10.3 ± 1.6	8.94 ± 0.29	12.2 ± 1.4	
$1.63\,10^{15}$	1835 Å[c]	4.75 ± 0.12	10.41 ± 0.29	5.60 ± 0.15	12.59 ± 0.35	
$2.05\,10^{15}$	1460 Å	3.43 ± 0.09	8.58 ± 0.23	4.21 ± 0.11	10.51 ± 0.28	
$2.19\,10^{15}$	1368 Å	...	...	3.92 ± 0.32	10.2 ± 0.83	
$2.26\,10^{15}$	1328 Å	...	...	3.46 ± 0.22	9.31 ± 0.60	
$2.56\,10^{15}$	1173 Å	...	...	3.04 ± 0.77	9.7 ± 2.4	
$2.77\,10^{15}$	1083 Å	...	...	18.4 ± 3.1	69 ± 12	
$3.12\,10^{15}$	963 Å	...	...	5.3 ± 2.5	26 ± 12	
$2.47\,10^{16}$	0.1 keV	...	...	~0.	0.0964[d,e]	
$2.47\,10^{17}$	1.0 keV	$4\,10^{-3}$ [f]	$5.2\,10^{-3}$ [f]	$2.07\,10^{-3}$ [e]	$2.62\,10^{-3}$ [d,e]	
$6.22\,10^{17}$	2.5 keV	$7\,10^{-3}$ [f]	$7.5\,10^{-3}$ [f]	$3.67\,10^{-3}$ [e]	$3.75\,10^{-3}$ [d,e]	
$2.42\,10^{19}$	0.1 MeV		$2.1 \pm 0.7\,10^{-4}$	...	...	

[a] Flux corrected for absorption by the interstellar medium in the Galaxy
[b] Not "pure" AGN, includes flux from the host galaxy
[c] F_ν(cor) has also been corrected for Fe II and Balmer continuum emission
[d] Flux uncorrected for the warm absorber contribution
[e] Flux on July 23, close to WAD secondary date
[f] Flux on the WAD primary date, as the flux on July 23 scaled according to the count-rate comparison (Sect. 2.8)

the first case, we extrapolate the X-ray based power law to lower energies and fit the spectrum after removal of the underlying power law. In the second case, we restrict the power-law component to the high-energy window. In both cases, two "bumps" appear, one in the UV (the "big blue bump") and one in the infrared, while the optical continuum point is almost at the level of the $\alpha = 1$ power-law extrapolation. The interpretation of these two bumps is not unambiguous and is beyond the scope of this paper (see for a brief review Shields & Peterson 1994). Therefore, in the following we present the results of comparing with a simple and commonly considered model, but without critical evaluation. In this model, the UV bump is interpreted as thermal emission from the accretion disc that is thought to surround a central massive black hole. The IR bump is considered to be re-radiation of UV flux absorbed by hot dust grains.

4.3.1. Power law plus thermal emission over the UV to mid-IR

We consider the UV bump to extend from 5150 Å up to the soft X-ray region at 0.1 keV. We attempt to fit a geometrically thin, optically thick accretion disc spectrum, computed in the Schwarzschild metric as a sum of blackbody spectra with full relativistic corrections (Lee et al. 1992). We sum the contributions from all annuli between 6 and 500 gravitational radii. We fit the model to the data obtained on the WAD secondary observation date using the data points from 1170 to 5150 Å. Free parameters in the fit are the power law normalization, the mass of the central black hole, and the accretion rate. The power-law spectral index is fixed at $\alpha = 1.0$. For a face-on disc (inclination of 0°) we find $M_{BH} = 2.0 \times 10^7\,M_\odot$ and an accretion rate of $0.015\,M_\odot yr^{-1}$. For a disc at an inclination of 60° we find $M_{BH} = 3.6 \times 10^7 M_\odot$ and an accretion rate of $0.023\,M_\odot yr^{-1}$. We can also consider the case of a face-on Kerr accretion disc. The power-law index is again fixed to a value of unity and its normalization is chosen to give a good match around the 5150 Å point and at slightly longer wavelengths where the disc contribution drops. The results for this model are $M_{BH} = 2.5 \times 10^7 M_\odot$, accretion rate $0.019\,M_\odot yr^{-1}$ and a power-law flux at $\nu = 5.5 \times 10^{14}$ Hz of 1.02×10^{28} erg s^{-1} Hz^{-1}. Figure 4 shows the results of the fit. In this approximation, the

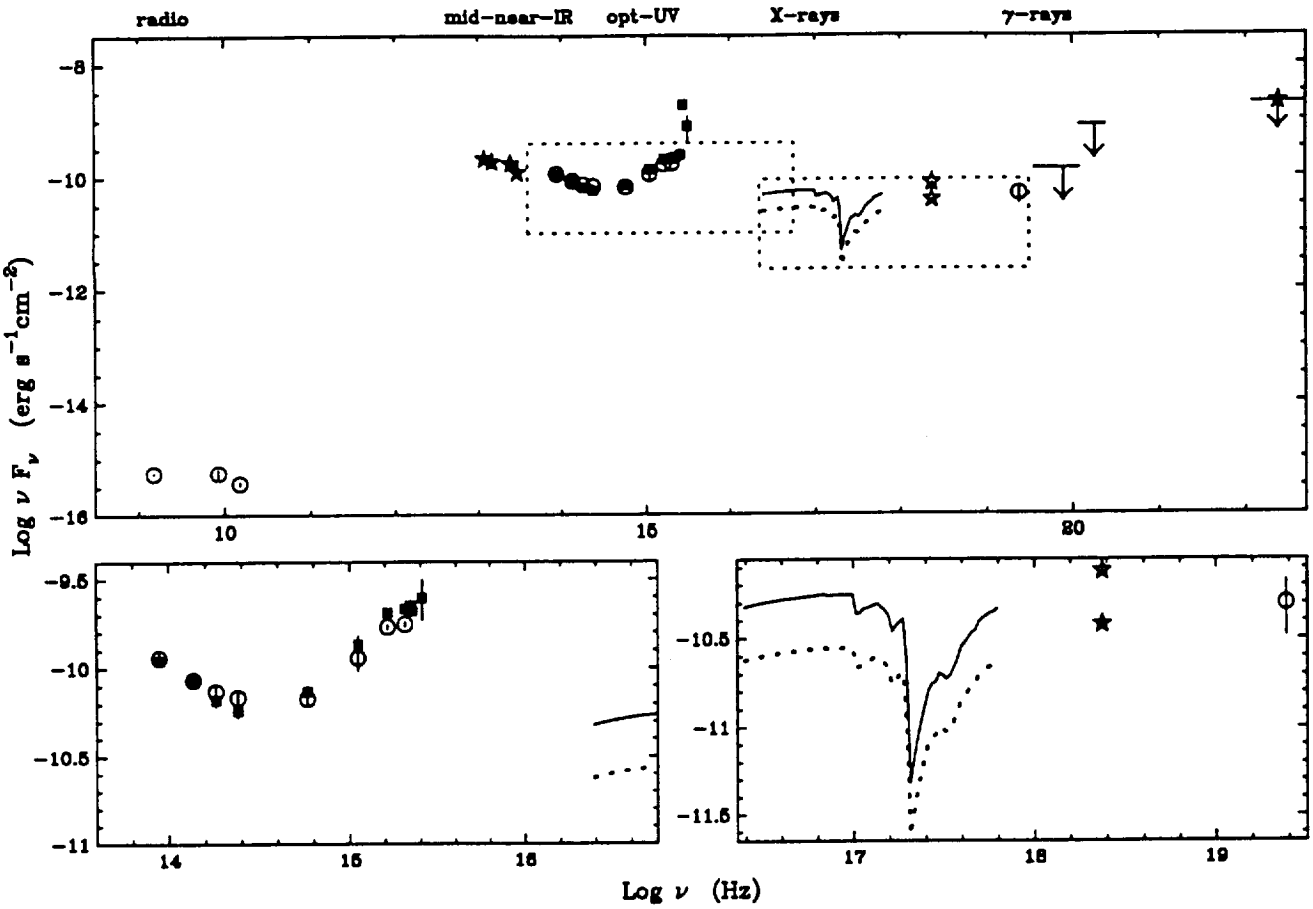

Fig. 3. The spectral energy distribution, corrected for absorption by neutral H in the line of sight, of the active nucleus in NGC 3783. Open circles represent data taken on 1992 June 29 – 30 (primary WAD date). Filled squares show data from 1992 July 27 – 28 (secondary WAD date). Stars are used for fluxes measured at earlier epochs (mid-IR points and high energy γ-ray point) or based on extrapolation (the hard X-ray points). The soft X-rays are represented by the fit to the data obtained close to the secondary WAD date (dotted line) and by a scaled similar model for the WAD primary date (continuous line), as explained in Sect 2.8. The optical-UV and X-rays domains have been enlarged in the lower frames

power law accounts for most of the optical nuclear flux, thus requiring the remaining blue bump to be very hot. Thus the highest disc temperatures are about 280,000 K. It must be noted that the optical–UV spectrum in NGC 3783, after the reddening correction, is rather flat (or blue), requiring high inner disc temperatures. This condition would have been relaxed, however, if we had fitted an extreme Kerr disc viewed at a fairly high inclination angle, in which case the accretion rate could be well below the Eddington rate, but the spectrum would be strongly blueshifted. Sun & Malkan (1989) give the exact formula for how the fitted black hole mass would have increased if the assumed inclination were increased from zero. An independent set of parameters has been derived by Rokaki et al. (1992) using another accretion disc model. They obtain, from a fit of the broad Hα and Hβ profiles and intensities and the UV continuum in NGC 3783 with emission from an accretion disc, $i = 25°$, $M_{BH} = 6 \times 10^7 M_\odot$, and two different values for the accretion rate depending on the assumed disc luminosity (either 0.028 or 0.009 $M_\odot yr^{-1}$).

Various accretion disc models lead to values of the black hole mass and accretion rate in NGC 3783 which are of the same order of magnitude. However, one should keep in mind the more fundamental limitations of the accretion disc modeling for AGN (Courvoisier & Clavel 1991)

In the near IR, the excess flux above the $\alpha = 1$ power law can be interpreted as a superposition of blackbody components arising in dust. The dust temperature ranges downward 1500 K (the average sublimation temperature of graphite and silicates) at a distance $r \approx 80 - 90$ light days, derived from variability arguments (Glass 1992). After subtraction of the underlying power-law flux, the residual 2.2 μm flux is ~34 mJy, and following Glass (1992) and Barvainis (1987), the total mass of hot grains emitting in the near IR can be estimated as $\sim 1.4 \times 10^{-3} M_\odot$. We can also tentatively estimate the mass of cooler dust which would explain the flux excess observed from 10 to 25 μm, again following Barvainis (1987). The properties of cool grains could be quite different from those of the hot grains radiating in the near IR, but as a first approximation, we assume that they have

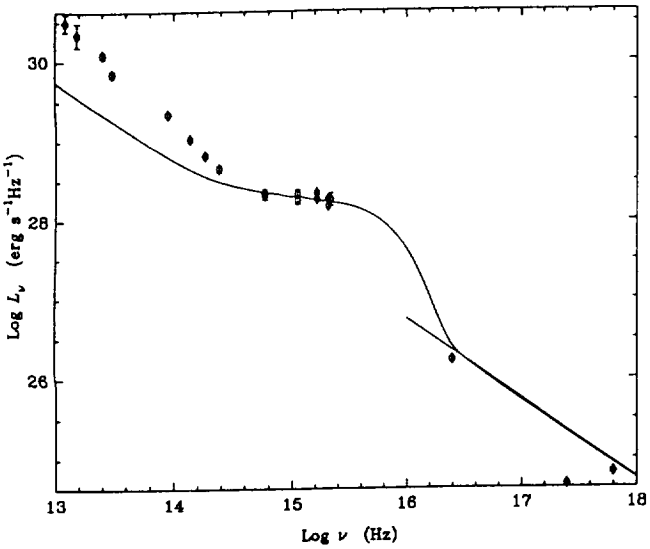

Fig. 4. The mid-IR to soft X-ray spectral energy distribution of NGC 3783. The continuous line is the sum of the Kerr accretion disc model plus the $\alpha = 1$ power law fitted to the mid and near IR, optical, UV and soft X-ray data points (see text; the Voyager points have been ignored). The straight line in the soft X-ray region is plotted to show where the high frequency power law is located

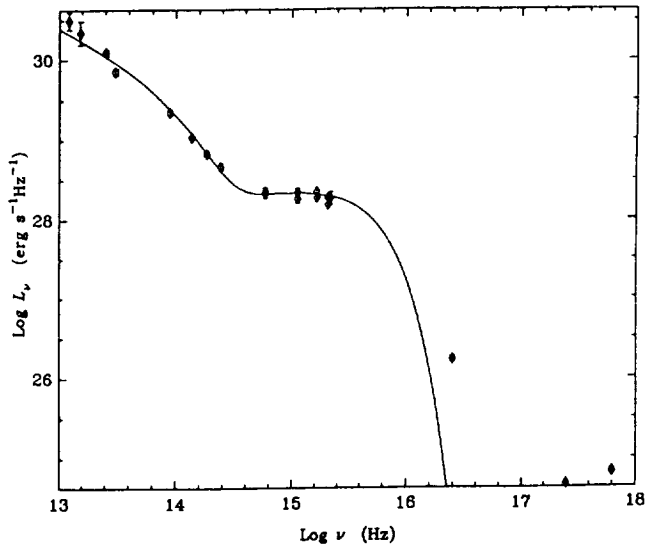

Fig. 5. The mid-IR to soft X-ray spectral energy distribution of NGC 3783. The continuous line represents the sum of the Kerr accretion disc model and heated dust emission fitted to the mid-and near IR, optical and UV data points (see text; the Voyager points have been ignored)

similar properties. The temperature of a blackbody that peaks at $\sim 25\,\mu$m in F_ν is ~ 200 K. At this temperature, the emissivity per grain is about 2.7×10^{-20} erg s^{-1} Hz^{-1} at 25 μm (Barvainis 1987). The observed flux at this frequency (after subtraction of the assumed underlying power law flux) is $\sim$1420 mJy, which requires a total mass in grains of $\sim 56\,M_\odot$. The grain temperature decreases with the distance to the UV emitting source as $T \propto r^{-2/5.6}$, assuming that the dust optical depth to the UV radiation remains constant. By combining this radial temperature dependence with the results from Glass (1992) that indicate that the warm ($T = 1500$ K) dust lies at a distance of $r \approx 85$ light days, we estimate that emission from the cool ($T = 200$ K) grains arises at a distance from the central source $r \approx 6.6 \times 10^{19}$ cm (i.e., 21 pc, with a corresponding angular size of 0".1 at the distance of NGC 3783).

4.3.2. Power law in the high energy domain, plus pure thermal UV to mid-IR emission

As an alternative, we consider the case where the X-ray power law does not extend to the optical and where the continuum emission in the UV and the IR is entirely of a thermal origin. The IR is again attributed to thermal dust re-radiation, and can be approximated by the analytic formula $L_\nu \propto \nu^{-0.7} e^{-\nu/(10^{14}\,\mathrm{Hz})}$, as discussed by Malkan (1992). In this case, the accretion disc must produce all of the optical and UV continuum flux. This can be done with approximately the same accretion rate as in the previous Kerr model ($0.019\,M_\odot \mathrm{yr}^{-1}$), but a larger black hole mass ($M_{BH} = 5 \times 10^7 M_\odot$) so that the innermost temperature is only about 210,000 K. In this case, the extension of the disc falls slightly below the observed 0.1 keV flux. The results are shown in Fig. 5. Since in this model the disc must produce all of the optical and UV flux, the model is much more tightly constrained than in the previous case considered. However, this simple thermal model for the accretion disc and dust component fails to explain by itself the origin of the hard X-rays and γ-rays.

This first-order exercise of fitting the spectral energy distribution of the AGN in NGC 3783 should be regarded as an illustration of the difficulty of the task, and of the uncertainties inherent to it. Complete and consistent modeling of the phenonemon is beyond the scope of this study and should incorporate as well constraints derived from the variability properties of the AGN (Paper V and Paper VI).

4.3.3. Concluding remarks

To first order, the nuclear spectral energy distribution of NGC 3783 is flat. If the $\alpha = 1$ power law that describes the high-energy domain (0.1 MeV – 0.1 keV) is extended into the UV and mid-IR domain, then there appear an excess of UV emission and also an excess of mid- to near-IR flux. The UV bump can be attributed to thermal emission from an accretion disc. The mass of the implied central black hole ($\sim 3 \times 10^7\,M_\odot$) and the disc accretion rate ($\sim 0.02\,M_\odot \mathrm{yr}^{-1}$) can be inferred by comparison with theoretical models of optically thick and geometrically thin discs. These are, of course, highly simplified models which in fact face severe problems when variability constraints are imposed. Modified or completely different scenarios (e.g., optically thin thermal emission) have been suggested to explain the UV bump. The results presented here thus should be considered as illustrative, and valid only within the context of the models in which they are derived. The IR bump is consistent with the presence of a dust component in the region extending

from 80 light days up to 60 light years away from the central engine, with temperatures in the range 1500 to 200 K. The total mass of dust required to explain the IR bump is $\sim 60\,M_{\odot}$. If the $\alpha = 1$ X-ray power law cannot be extrapolated to longer wavelengths, both the UV and IR bumps can still be explained in terms of an accretion disc and dust components, but with larger black hole mass and dust content.

Acknowledgements. We are gratefully indebted to R.M. Catchpole and C.D. Laney for obtaining the near-IR data at SAAO. We wish to warmly thank R. Booth, R. Costero, R. Giacconi, J.D. Kurfess, R. Lopez and J. Melnick for supporting this campaign. We also acknowledge the support of all staff at the various facilities used during the campaign. Finally, we are grateful to the following agencies for direct support of these observations: NASA (grants NAG5-1824 and NAGW-3315 to Ohio State University), ESA, ESO and NOAO.

References

Agayev A.G., Guseinov O.H., & Novruzova H.I., 1982, Ap&SS 81, 5
Alloin D., Clavel J., Peterson B.M., Reichert G.A. & Stirpe G.M., 1994. In: Wamsteker W., Longair M.S., Kondo Y., (eds.) Frontiers of Space and Ground-Based Astronomy. Kluwer, Dordrecht p. 325
Baars J.W., Genzel R., Pauliny-Toth I.I., & Witzel A., 1977, A&A 61, 99
Baribaud T., Salamanca I., Alloin D., & Wagner S., 1994, A&AS 103, 121
Barr P., Willis A.J., & Wilson R., 1983, MNRAS 202, 453
Barvainis R., 1987, ApJ 320, 537
Bica E., 1988, A&A 195, 76
Bica E., & Alloin D., 1988, A&A 192, 98
Broadfoot A.L., Sandel B.R., Shemansky D.E., et al., 1977, Space Sci. Rev., 21, 183
Burstein D., & Heiles C., 1982, AJ 87, 1165
Carter B.S., 1990, MNRAS 242, 1
Chapman G.N., Geller M.J., & Huchra J.P., 1985, ApJ 297, 151
Clavel J., Boksenberg A., Bromage G., et al., 1990, MNRAS 246, 668
Clavel J., Reichert G., Alloin D., et al., 1991, ApJ 366, 64
Courvoisier T. & Clavel J., 1991, A&A 248, 389
Dietrich M., Kollatschny W., Peterson B.M., et al., 1993, ApJ 408, 416
Evans I.N., 1989, ApJ 338, 128
Frogel J.A., Elias J.H., & Phillips M.M., 1982, ApJ 260, 70
Gehrels N., Chipman E. & Kniffen D.A., 1993, AIP Conf. Proc. 280, p. 3
Ghosh K.A., Soundararajaperumal S., Kalai Selvi M., & Sivarani T., 1992, A&A 255, 119
Glass I.S., 1973, MNRAS 164, 155
Glass I.S., 1984, MNRAS 211, 461.
Glass I.S., 1985a, MNRAS 44, 45
Glass I.S., 1985b, Irish AJ, 17, 1
Glass I.S., 1992, MNRAS 256, 23P
Glass I.S., Moorwood A.F.M. & Eichendorf W., 1982, A&A 107, 276
Hasinger G., Turner T.J., George I.M., & Boese G., 1992, Legacy 2, 77 (OGIP Calibration Memo CAL/ROS/92-001)
Holberg J.B., Forrester W.T., Shemansky D.E. & Barry D.C., 1982, ApJ 257, 656
Holberg J.B., Ali B., Carone T.E., & Polidan R.S., 1991, ApJ 375, 716
Johnson W.N., Kinzer R.L., Kurfess J.D., et al., 1993, ApJS, 86, 693
Johnson W.N., Grove J.E., Kinzer R.L., et al., 1994, In: 2nd Compton Symposium, in press
Klare G. & Szeidl B., 1966, Landessternwarte Heidelberg Konigstuhl Veroffentlichungen 18, 9
Kotilainen J.K., Ward M.J., & Williger G.M., 1993, MNRAS 263, 655
Krolik J. H., & Begelman M. C., 1986, ApJ 308, L55
Lee G., Kriss G. A. & Davidsen A. F., 1992, Testing the AGN Paradigm. In: Holt S.S., Neff S.G., Urry C.M. (eds.) AIP, New York, p. 159
Lin Y.C., Bertsch D.L., Dingus B.L., et al., 1993, ApJ 416, L53
Luyten W.J., 1977, University of Minnesota Press
Malkan M., 1992, Physics of Active Galactic Nuclei. In: Duschl W.J., Wagner S.J. (eds.) Proc. of the International Conference, Heidelberg, June 1991.,Springer-Verlag, Berlin, Heidelberg, p. 109
Marshall N., Warwick R.S., & Pounds K.A., 1981, MNRAS 194, 987
McHardy I., 1988, Mem. Soc. Astron. Ital. 59, 239
Menzies J.W., & Feast M.W., 1983, MNRAS 203, 1P
Maoz D., Netzer H., Peterson B.M., et al., 1993, ApJ 404, 576
Napier P.J., Thomson A.R., & Eckers R.D., 1983, Proc. IEEE 71, 1295
Netzer H., 1993, ApJ 411, 594
Pelat D., Alloin D., & Fosbury R.A., 1981, MNRAS,195, 787
Peterson B.M., 1993, PASP 105, 247
Peterson B.M., Alloin D., Axon D., et al., 1992, ApJ 392, 470
Peterson B.M., Balonek T.J., Barker E.S., et al., 1991, ApJ 368, 119
Peterson B.M., Berlind P., Bertram R., et al., 1994, ApJ 425, in press
Pfeffermann E., Briel U.G., Hippman H., et al., 1986, Proceedings SPIE, 733, 519
Reichert G.A., Mushotzsky R.F., Petre R., & Holt S.S., 1985, ApJ 296, 69
Reichert G.A., Rodríguez-Pascual P.M., Alloin D., et al., 1994, ApJ 425, in press (Paper V)
Roche P.F., Aitken D.K., Smith C.H., & Ward M.J. 1991, MNRAS 248, 606
Rokaki E., Boisson, C.,& Collin-Souffrin, S. 1992, A&A, 253, 57
Santos-Lleó M., Alloin D., 1995, in preparation
Schroder M.F.S., & Kepler S.O., 1991, PASP 103, 383
Shields J.C., & Peterson B.M., 1994, Comments on Astrophysics, 17, 241
Seaton M.J., 1979, MNRAS 187, 73P
Stark A.A., Gammie C.F., Wilson R.W., et al., 1992, ApJS 78, 77
Stirpe G.M., de Bruyn A.G., & van Groningen E. 1988, A&A 200, 9
Stirpe G.M., Winge C., Altieri B., et al., 1994, ApJ 425, in press (Paper VI)
Sun W.H., Malkan M.A., 1989, ApJ 346, 68
Turner T.J., Nandra K., George I.M., Fabian A.C., & Pounds K.A., 1993, ApJ 419, 127
Turner T.J., Weaver K.A., Mushotzsky R.F., Holt S.S. & Madejski G.M., 1991, ApJ 381, 85
Trümper J., 1983, Adv. Space Res., 2, 241
Wamsteker W., Rodríquez-Pascual P.M., Wills B.J., et al., 1990, ApJ 354, 446
Ward M., Elvis M., Fabbiano G., et al., 1987, MNRAS 315, 74
Wills B.J., Netzer H., Wills D., 1985, ApJ 288, 94
Winge C., Pastoriza M.G., Storchi-Bergmann T. & Lipari S., 1992, ApJ 393, 98
Winkler H., Glass I.S., van Wyk F., et al., 1992, MNRAS 257, 659
Yaqoob T. & Warwick R.S., 1991, MNRAS 248, 773

This article was processed by the author using Springer-Verlag LaTeX A&A style file version 3.